

1 **Bulk meltwater flow and liquid water content of snowpacks**
2 **mapped with the electrical self-potential (SP) method**

3

4 S. S. Thompson^{1,*}, B. Kulesa², R. L. H. Essery³, M. P. Lüthi^{4,*}

5 (1) Department of Arctic Geology, University Centre in Svalbard (UNIS), Svalbard

6 (2) College of Science, Swansea University, UK

7 (3) The School of Geosciences, University of Edinburgh, UK

8 (4) University of Zurich, Switzerland

9 (*) Formerly at Versuchsanstalt für Wasserbau, Hydrologie und Glaziologie (VAW), ETH
10 Zürich, Switzerland

11 Correspondence to S. S. Thompson (Sarah.Thompson@unis.no)

12

13 **ABSTRACT**

14 Our ability to measure, quantify and assimilate hydrological properties and processes of snow
15 in operational models is disproportionately poor compared to the significance of seasonal
16 snowmelt as a global water resource and major risk factor in flood and avalanche forecasting.
17 We show here that strong electrical self-potential fields are generated in melting in-situ
18 snowpacks at Rhone Glacier and Jungfrauoch Glacier, Switzerland. In agreement with theory
19 the diurnal evolution of self-potential magnitudes ($\sim 60 - 250$ mV) relates to those of bulk
20 meltwater fluxes ($0 - 1.2 \times 10^{-6} \text{ m}^3 \text{ s}^{-1}$) principally through the permeability and the content,
21 electrical conductivity (EC) and pH of liquid water. Previous work revealed that when fresh
22 snow melts, ions are eluted in sequence and EC, pH and self-potential data change
23 diagnostically. Our snowpacks had experienced earlier stages of melt, and complementary
24 snow pit measurements revealed that EC ($\sim 1.5 \times 10^{-6} \text{ S m}^{-1}$) and pH ($\sim 6.5 - 6.7$) as well as

25 permeabilities (respectively $\sim 9.7 \times 10^{-5} \text{ m}^2$ and $\sim 4.3 \times 10^{-5} \text{ m}^2$ and Rhone Glacier and
26 Jungfrauoch Glacier) were invariant. This implies, first, that preferential elution of ions was
27 complete and, second, that our self-potential measurements reflect daily changes in liquid water
28 contents. These were calculated to increase within the pendular regime from $\sim 1 - 5 \%$ and \sim
29 $3 - 5.5 \%$ respectively at Rhone Glacier and Jungfrauoch Glacier, as confirmed by ground
30 truth measurements. We conclude that the electrical self-potential method is a promising snow
31 and firn hydrological sensor owing to its suitability for [1] sensing lateral and vertical liquid
32 water flows directly and minimally invasively, [2] complementing established observational
33 programs through multidimensional spatial mapping of meltwater fluxes or liquid water
34 content, and [3] low-cost autonomous monitoring. Future work should focus on the
35 development of self-potential sensor arrays compatible with existing weather and snow
36 monitoring technology and observational programs, and the integration of self-potential data
37 into analytical frameworks.

38

39 **1. Introduction**

40 More than a sixth of the world's population relies on melt from seasonal snow and glaciers for
41 water supply (Barnett et al., 2005). Snow, and runoff from snow, are also major resources for
42 the hydroelectric, tourism and inland fishery industries, and furthermore represent hazards from
43 flooding and avalanches (Mitterer et al., 2011). The availability of snow models constrained
44 by a reliable observational basis, for the forecasting of snow hydrological properties and
45 processes in climate, resource and hazard applications is therefore of considerable socio-
46 economic significance (Wever et al., 2014). However, the parameterisation of fundamental
47 snow-hydrological attributes, such as liquid water content and flux, is a well-recognised major
48 source of uncertainty in operational models used in snow and hydrological forecasting (Livneh
49 et al., 2010, Essery et al., 2013). This uncertainty in operational models is rooted principally in

50 the inability of traditional snow-hydrological techniques to provide automated attribute
51 measurements non-invasively and on spatial scales that match those used in operational snow
52 models. Relevant traditional techniques include dielectric (Denoth, 1994) or ‘hand’ tests (Fierz
53 et al., 2009) of snow liquid water contents, lysimeter measurements of discharge, temperature
54 and pH and electrical conductivity of bulk meltwaters (Campbell et al., 2006, Williams et al.,
55 2010), and manual observation or measurement of snow density and grain size (Fierz et al.,
56 2009). Even cutting edge upward-looking radar measurements of snowpack structure and
57 liquid water content (Heilig et al., 2010; Mitterer et al., 2011; Schmid et al., 2014) compare
58 unfavourably with model predictions of wetting front propagation (Wever et al., 2014),
59 attributed to inherent limitations of 1-D approach in capturing preferential flow.

60 By combining field measurements with a theory and model of self-potential signals
61 associated with unsaturated flow in melting snow (Kulesa et al. 2012), we show here that
62 electrical self-potential geophysical data integrated with traditional snow measurements can
63 address these limitations. The self-potential technique is a passive geo-electrical method that
64 exploits the presence of naturally-occurring electrical potentials in the subsurface generated as
65 a result of dipolar charge separation when water flows through a porous matrix (‘streaming
66 potential’; Darnet et al., 2003, Revil et al., 2006). The self-potential method has a unique
67 ability in delineating, monitoring, and quantifying the flow of subsurface water in groundwater
68 aquifers and unsaturated media (e.g., Revil et al., 2006, and references therein), and for
69 numerous cold regions application (e.g., French et al., 2006; Kulesa, 2007, and references
70 therein). This ability is due on the fact that pore waters generally have an excess of electrical
71 charge due to the electrical double layer at the interface between the solid matrix (in this case
72 snow grains) and pore water. The advective drag of this excess of electrical charge is
73 responsible for a streaming current, whose divergence generates a quasistatic electric field
74 known as the streaming potential (Sill, 1983; Revil et al., 2003). More recently, streaming

75 potential theory has been extended for unsaturated conditions (Linde et al., 2007; Revil et al.,
76 2007; Jougnot et al., 2012). A new theory and numerical model of self-potential signals
77 associated with unsaturated flow in melting snow, along with laboratory tests, strongly
78 promoted the technique as a non-intrusive hydrological sensor of water fluxes (Kulesa et al.,
79 2012) at spatial scales intermediate between snow pits and satellite footprints or, given
80 independent flux measurements, of evolving physical and chemical properties of snow and
81 snow-melt.

82 We answer two fundamental questions: 1) Can the self-potential method serve as a non-
83 intrusive field sensor of temporally evolving bulk meltwater fluxes and liquid water contents
84 of snow? 2) What are the ambiguities introduced into estimates of liquid water contents from
85 self-potential and bulk discharge data, by uncertainties inherent in the governing snow physical
86 and chemical properties? Lastly we discuss the implications and possibilities of the technique
87 for future snow measurement and modelling research and practice. Our study thus takes a
88 significant step towards the in-situ implementation of the self-potential method for improved
89 characterization and monitoring of snow liquid water contents and melt water fluxes.

90

91 **2. Theory, field sites and methods**

92 The Poisson equation relates the electrical field ψ to the source current density in a partially
93 or fully-saturated snow pack,

94

$$\nabla \cdot (\sigma \nabla \psi) = \nabla \cdot \mathbf{j}_s, \quad (1)$$

95

96 where σ is the bulk electrical conductivity of the porous material (in S m^{-1}), and \mathbf{j}_s is the source
97 current density (in A m^{-2}). Equation (1) applies only in the low-frequency limit of the
98 Maxwell's equations without external injection or retrieval of charges, or charge storage in the

99 snowpack. Extending the classic Helmholtz-Smoluchowski theory for unsaturated flow in
100 snow, the one-dimensional solution to equation (1) is given by

101

$$\psi_m - \psi_0 = -\frac{\varepsilon\zeta}{\eta\sigma_w} S_w (H_m - H_0), \quad (2)$$

102

103 where ψ_m and H_m are respectively the electrical and hydraulic potentials at the measurement
104 electrode, ψ_0 and H_0 are the corresponding potentials at the reference electrode, ζ is the zeta
105 potential (V), and ε , η , σ_w and S_w are respectively the dielectric permittivity (F m^{-1}), dynamic
106 viscosity (in Pa s), electrical conductivity (S m^{-1}) and relative saturation (dimensionless) of the
107 melt or rainwaters in the snowpack's pore space (Kulesa et al., 2012). The zeta potential is the
108 voltage across the electrical double layer at the interface between the ice matrix and the pore
109 waters, as controlled by these constituents' physical and electrical properties.

110 To address the specific objectives set out in the introduction through data-driven testing,
111 we developed an experimental survey design to simulate the geometry of Kulesa et al.'s (2012)
112 laboratory snow column (Fig. 1b). It was therefore our aim to characterise lateral-bulk
113 meltwater fluxes in inclined snowpacks at two glaciers in Valais, Switzerland, measuring all
114 relevant snow pack attributes for ground truth. Self-potential and traditional snow-hydrological
115 measurements were acquired on 13th, 14th and 15th June 2013 from the ablation area snowpack
116 at Rhone Glacier, and 5th September 2013 from the glacial accumulation area at Jungfrauoch
117 Glacier (Fig.1a). At Rhone Glacier and Jungfrauoch Glacier site elevations were respectively
118 2340 and 3460 m.asl., with surface gradients of $\sim 8^\circ$ and 17° . At the Rhone Glacier all three
119 days experienced comparable air temperature, although 15th June was noticeably cloudier with
120 a very low sunshine duration. Because daily average temperatures were between 5 and 15 °C

121 with no fresh snowfall (MeteoSuisse), the snowpacks would have experienced significant
122 melting in the weeks before the surveys. We therefore expect them to be physically mature in
123 terms of enhanced grain size and density due to metamorphosis, and chemically mature in terms
124 of invariant meltwater pH and electrical conductivity as preferential elution of solutes has been
125 completed (Kulesa et al., 2012, and references therein).

126 At both sites more than 100 self-potential measurements were made at the snow surface,
127 and meltwater bulk discharge in a lysimeter, pH and electrical conductivity, and snowpack
128 characteristics including thickness, density, grain size and liquid water content were recorded.
129 Adopting our established acquisition procedures (Thompson et al., 2012), we conducted all
130 self-potential surveys using a pair of lead/lead chloride ‘Petiau’ non-polarising electrodes
131 (Petiau, 2000). The survey was carried out following the potential amplitude method (Corry et
132 al., 1983); this employs a reference electrode in a fixed location and a roving electrode which
133 is moved through the survey area at 0.5 m intervals (Fig.1a). Self-potential surveys were
134 conducted in profiles of 25 data points perpendicular to the principal direction of water flow,
135 where the latter was assumed to follow the gradient indicated by snow surface topography. All
136 self-potential measurements were taken as differential readings relative to the reference
137 electrode, minimizing streaming, electrochemical and thermal potentials at the latter by
138 grounding them outside the survey areas at the top of a local topographic high point (Fig. 1a),
139 submerged in a glass jar, open at the top and filled with water-saturated local media (Kulesa
140 et al., 2003a). The jar was then buried upright ~1 m deep to avoid exposure to surface
141 temperature variations. Surveys were carried out with a fixed tie-in point (measured every
142 second line) at the reference electrode, allowing for correction of the effects of electrode
143 polarisation and drift (Doherty et al., 2010, Thompson et al., 2012).

144 Bulk discharge through a snowpack is preferably measured with a lysimeter (Campbell
145 et al., 2006, Williams et al., 2010), in this case made up of a series of smaller (guttering) areas

146 joined together to prevent freezing and compaction (after Campbell et al., 2006). The lysimeter
147 was placed at the base of Rhone Glacier's snowpack, and at the limit of the diurnal melt
148 penetration depth at Jungfrauoch Glacier (determined by daily dye tracing experiments). Snow
149 density (by balance) and average snow grain size (crystal card and lens) were measured, at the
150 start and end of each self-potential survey to reveal any intermittent snow metamorphism, using
151 standardised techniques within the top and basal layers of snow pits freshly excavated at the
152 survey sites (Fierz et al., 2009). Liquid water content was estimated using two different
153 techniques, including the hand test (Colbeck et al., 1990, Fierz et al., 2009) in the surface and
154 base layers of Rhone Glacier's snow pit, and the Denoth Capacitance Meter (Denoth, 1994) in
155 the surface and base layers of the snow pit at Jungfrauoch Glacier. The latter were acquired
156 across a 2D grid where the instrument was inserted into the snowpack at a depth of 0.4 m
157 following the same survey spacing as the self-potential measurements.

158

159 **3. Field measurement results**

160 The drift-corrected self-potential magnitudes and meltwater bulk discharges both increase with
161 time through the day until a peak in late afternoon, after which they both begin to decrease
162 (Fig. 2). There is no distinguishable time lag between the measured self-potential magnitude
163 and discharge data (Fig. 2), and the ratio between self-potential and bulk discharge changes
164 consistently over time (Fig.3). Days 1 and 2 at Rhone Glacier were characterised by higher
165 discharges and self-potential magnitudes compared to day 3, and intriguingly bulk discharge
166 at Jungfrauoch Glacier was akin to day 3 at Rhone Glacier but self-potential magnitudes at
167 Jungfrauoch Glacier were much higher than days 1 and 2 at Rhone Glacier (Fig. 2). The pH,
168 electrical conductivity and temperature of meltwater, recorded with each bulk discharge
169 measurement, show no consistent temporal or spatial variation across any of the four field
170 surveys. Fluid electrical conductivity values generally ranged between $1 \times 10^{-6} \text{ S m}^{-1}$ and $5 \times$

171 10^{-6} S m^{-1} without spatial or temporal consistency, while pH ranged between 6.5 and 6.9. Snow
172 grain size remained constant at $\sim 1.5 \text{ mm}$ at Rhone Glacier and $\sim 1 \text{ mm}$ at Jungfrauoch Glacier,
173 while snow densities ranged between 555 kg m^{-3} and 573 kg m^{-3} without spatial or temporal
174 consistency. The very small variability range of the snowpack characteristics measured is
175 consistent with mature snowpacks, as assumed above with reference to prior meteorological
176 conditions. At Rhone Glacier the liquid water content of snow had a wetness index of 3
177 irrespective of measurement time or location at the surface or base of the snow pit, associated
178 with a liquid water content range of 3 – 8 % vol. (Colbeck et al., 1990). At Jungfrauoch Glacier
179 liquid water content, measured using the Denoth meter, gave profile-averaged values of 1.5 to
180 $\sim 5.0 \text{ % vol.}$, increasing consistently throughout the survey period. These measurements and
181 inherent uncertainties are used below for snow liquid water content calculations, uncertainty
182 analysis and sensitivity testing.

183

184 **4. Objective 1: Self-potential as a snow-hydrological sensor**

185 Both survey areas were south facing, topographically-inclined but otherwise had no visibly
186 distinguished snow surface undulations, and any snow thickness variations were minimal. We
187 therefore expect changes in self-potential magnitudes to be pronounced in the downslope
188 direction, and minimal across-slope along any individual profile (Fig. 1a). Averaging all 25
189 self-potential data points acquired along any particular profile, a one-dimensional upslope-
190 downslope series of self-potential magnitudes is produced for a given survey area on a given
191 day, together with uncertainty estimates reflecting natural spatial and temporal variability along
192 the profile (Supporting Information). For each profile the acquisition time of the central data
193 point was assigned to it, and all measurements of snowpack and meltwater properties were
194 averaged over the same time period ($\sim 20 \text{ mins}$, i.e. the acquisition time of any one self -
195 potential profile). The upslope-downslope series of average self-potential magnitudes thus

196 emulates measurements along a horizontally inclined version of the one-dimensional snow
197 column used in Kulesa et al. (2012) (Fig. 1b). These authors reformulated the one-dimensional
198 solution in equation (2) to relate measured self-potential magnitudes and bulk discharges
199 through their partially saturated snow column, which we can therefore adapt here to our field
200 experiment.

201 This adaptation is dependent on four key assumptions, including; 1) water flow within
202 the survey areas' snowpacks is laminar and homogenous in three dimensions, where snowpack
203 surface and base have constant and equal inclination and thus maintain a spatially constant
204 hydraulic gradient; 2) all contributions to the measured self-potential signal from flow below
205 the base of the snowpack, runoff at the surface of the snowpack, and flow outside the lateral
206 boundaries of the survey areas' snowpacks are negligible, and all water contributing to the
207 measured self-potential signals is adequately captured by our bulk discharge measurements; 3)
208 all snow physical and chemical properties controlling the self-potential magnitude do not vary
209 spatially across the survey areas' snowpacks, so that our ground-truth snow-pit data apply
210 uniformly across them, and 4) any spatial changes in self-potential magnitudes are dominated
211 by temporal changes in snow or meltwater properties, while static elevation driven spatial
212 changes are negligible. We assess the implications of any potential violations to these
213 assumptions in Section 6.

214 At a given time, t_n , the measured self-potential field, $\Psi_m(t_n)$, in our survey area is the
215 difference between the locally produced self-potential field, $\Psi_l(t_n)$, and the self-potential field
216 at the reference electrode, $\Psi_0(t_n)$. The latter is unknown in our field feasibility study, although
217 our method of emplacing the reference electrode is elaborate and designed to eliminate, or at
218 least minimise, any streaming potentials at the reference electrode ([see Section 2](#)). Once the
219 reference electrodes have settled in their environments, we further expect any electrochemical
220 or thermal potentials to be negligible. We can therefore expect $\Psi_0(t_n)$ to be close to zero, but

221 nonetheless apply caution and take a two-step approach. Initially we eliminate the reference
 222 self-potential fields by considering temporal changes in measured self-potentials only before,
 223 subsequently, considering absolute self-potential magnitudes.

224

225 ***Temporal changes in self-potential magnitudes.***

226 We can eliminate the reference field by differencing two self-potential measurements acquired
 227 at two successive times:

228

$$\psi_m(t_n) - \psi_m(t_{n-1}) = \psi_l(t_n) - \psi_l(t_{n-1}) \quad (3)$$

229

230 Equation (3) assumes that Ψ_0 and H_0 are temporally invariant, a reasonable supposition for
 231 drift-corrected self-potential data if the reference electrode is correctly emplaced. Recognising
 232 that $\psi_0 = H_0 \approx 0$ for their snow column experiment, Kulesa et al. (2012) reformulated equation
 233 (2) to show that the self-potential field at a measurement electrode, $\psi_l(t_n)$, can be approximated
 234 by

235

$$\psi_l(t_n) = \frac{\varepsilon \zeta}{\sigma_w} \frac{S_w(t_n)}{S_e^n(t_n)} \frac{1}{kA} Q(t_n) \quad (4)$$

236

237 where Q ($\text{m}^3 \text{s}^{-1}$) is bulk discharge in the snow pack through cross-sectional area A (m^2), k is
 238 permeability, S_e is effective saturation and $n \approx 3.3$ is the saturation exponent (after Albert et
 239 al., 1998, Kulesa et al., 2012). Assuming that any temporal changes in the self-potential field
 240 at the reference electrodes in our field experiments are negligible, the difference between
 241 successive field self-potential measurements in time can be approximated by

242

$$\psi_m(t_n) - \psi_m(t_{n-1}) = \frac{\varepsilon \zeta}{\sigma_w} \frac{1}{kA} \left(\frac{S_w(t_n)}{S_e^n(t_n)} Q(t_n) - \frac{S_w(t_{n-1})}{S_e^n(t_{n-1})} Q(t_{n-1}) \right) \quad (5)$$

243

244 In the present case we have measured $\Psi_m(t_n)$ and $\Psi_m(t_{n-1})$ as well as $Q(t_n)$ and $Q(t_{n-1})$. We have
 245 also measured, or can estimate from well-established empirical relationships, all other
 246 parameters coupling the temporal difference in self-potential fields ($\Psi_m(t_n)$ and $\Psi_m(t_{n-1})$) to that
 247 of discharge (expression in the large parentheses on the right-hand side of equation(5)). To
 248 demonstrate the usefulness of self-potential measurements in snow research and practice, we
 249 can therefore evaluate equation (5) at successive times, t_n and t_{n-1} , to calculate temporal changes
 250 in the liquid water content, S_w , of the snowpacks at our field sites. This evaluation is subject to
 251 assumptions (1) to (4) above, and is ground-truthed using snow pit measurements of liquid
 252 water contents.

253 At both Rhone Glacier and Jungfraujoeh Glacier self-potential magnitude (Ψ_m), bulk
 254 discharge (Q), electrical conductivity (σ_w) and cross-sectional area (A) (survey area width \times
 255 snow depth) were measured directly. Assuming that water at 0 °C has a dielectric permittivity
 256 of $\varepsilon_r = 88$, the dielectric permittivity ($F\ m^{-1}$) of pore meltwater is $\varepsilon = \varepsilon_r \varepsilon_0 = 7.8 \times 10^{-9}\ F\ m^{-1}$,
 257 where $\varepsilon_0 = 8.85 \times 10^{-12}\ F\ m^{-1}$ is the dielectric permittivity of vacuum. Permeability (k) can be
 258 derived from our snow density (ρ_s) and grain size (d) measurements using Shimizu's (1970)
 259 empirical relationship

260

$$k = 0.077 d^2 e^{-0.0078 \rho_s} \quad (6)$$

261

262 where k is in m^2 , d is in m and ρ_s in $kg\ m^{-3}$. This commonly used equation was derived from a
 263 fit to laboratory data collected with small rounded grains and a starting grain diameter of ~ 0.33
 264 mm (Shimizu, 1970). However, later work ascertained experimentally that Shimizu's [1970]

265 empirical formula does in fact apply to a much larger range of grain diameters, as expected to
266 be encountered in practice (less than 0.33 mm to greater than 2 mm) (Jordan et al., 1999). We
267 can therefore expect equation (6) to be robust for our purposes. Effective saturation (S_e) and
268 S_w are related through the irreducible water saturation S_w^{ir} by

$$S_e = \frac{S_w - S_w^{ir}}{1 - S_w^{ir}} \quad (7)$$

270
271 In the absence of direct measurements we adopt the commonly used values of $S_w^{ir} = 0.03$ and n
272 ≈ 3.3 (Kulesa et al., 2012), and assume that these values are invariant in space and time at our
273 study sites.

274 A significant challenge arises however in that there is one remaining parameter, the
275 zeta potential (ζ), which is unknown here and poorly constrained in general. Earlier work on
276 artificial ice samples, of fixed bulk electrical conductivity, ascertained that the zeta potential
277 reverses sign from $\sim +0.01$ V to ~ -0.02 V as equilibrium pH increases from less than 3 to
278 greater than 8 (Drzymala et al., 1999, Kallay et al., 2003). The electrochemical properties of
279 the electrical double layer at the snow grain surfaces, and thus also the magnitude and
280 potentially the sign of the zeta potential, will change over time in a fresh snowpack as the snow
281 is affected by melt, recrystallisation and the preferential elution of ions (Meyer and Wania,
282 2008, Meyer et al., 2009, Williams et al., 1999). Recent ‘natural snowmelt’ laboratory
283 experiments were consistent with a progressive increase of pH from 4.3 to 6.3 and a
284 simultaneous decrease in electrical conductivity from $\sim 1 \times 10^{-1}$ S m⁻¹ to $\sim 6 \times 10^{-7}$ S m⁻¹, as
285 the elution of ions follows a well-known sequence (Kulesa et al., 2012)). Upon conclusion of
286 the Kulesa et al.’s (2012) laboratory experiments, modelled rates of change of pH and
287 electrical conductivity were minimal and the snow column mature. The zeta potential is

288 principally a function of pH and electrical conductivity and the combined dependency of the
289 zeta potential on EC (sw), meltwater pH (pHw) and the meltwater pH at the point of zero charge
290 (pHw (pzc)) can be expressed as
291

$$\zeta(\sigma_w, pH) = [\alpha + \beta \log_{10} \sigma_w] \left(\sin \frac{\pi}{12} [pH_w - pH_w(pzc)] \right), \quad (8)$$

292
293 where α and β depend on the chemical composition of the pore fluid and can be determined
294 empirically (Revil et al., 1999). Kulesa et al. (2012) inferred the zeta potential changed from
295 $\sim -7.5 \times 10^{-2}$ V at the start of the natural snowmelt experiments to $+1.5 \times 10^{-2}$ V at the end,
296 when the rate of change of the zeta potential was minimal.

297 The final values of pH and electrical conductivity that Kulesa et al. (2012) calculated
298 from equation 8 were similar to those measured at Rhone Glacier and Jungfrauoch Glacier
299 (respectively $\sim 6.5 - 6.9$ and $\sim 1 - 5 \times 10^{-6}$ S m⁻¹), suggesting that these in-situ snow packs
300 were likewise mature as expected (Section 2). This inference is corroborated by the absence of
301 consistent spatial or temporal changes in either pH or electrical conductivity throughout the
302 survey periods. In Kulesa et al.'s (2012) laboratory study, the pH-corrected zeta potential had
303 values around zero for the range of electrical conductivities ($1 - 5 \times 10^{-6}$ S m⁻¹) measured at
304 Rhone Glacier and Jungfrauoch Glacier ($1 - 5 \times 10^{-6}$ S m⁻¹), and its rate of change became
305 minimal along with those of pH and electrical conductivity. We can therefore expect a small
306 and invariant zeta potential value to apply to the snowpacks at Rhone Glacier and Jungfrauoch
307 Glacier. Indeed, an excellent fit ($R^2 \approx 0.85$) between liquid water contents measured at
308 Jungfrauoch Glacier with the Denoth meter and that calculated based on equation (5) is
309 obtained when the zeta potential is assigned a value of $\sim -1 \times 10^{-5}$ V (Fig. 4). This excellent fit
310 suggests that in-situ measurements or empirically derived estimates of the parameters affecting

311 coupling between measured self-potential magnitudes and discharges in equation (5) are robust
312 for practical purposes.

313

314 *Absolute changes in self-potential magnitudes.*

315 The same parameters affect the coupling between temporal changes in self-potential
316 magnitudes and discharge (equation 5), and absolute changes therein as described by equation
317 (4) derived by assuming that the reference potential is zero. We are therefore encouraged to
318 calculate absolute liquid water contents from our self-potential data using equation (4). We do
319 this initially for Jungfrauoch Glacier because here we have detailed ground-truth
320 measurements of liquid water content made with a Denoth meter. Encouragingly we find that
321 calculated and measured ground-truth data match each other very well (Fig. 5a), attesting to
322 the fact that the reference potentials at Jungfrauoch Glacier may not only be temporally
323 invariant as confirmed earlier, but generally have negligible magnitudes.

324 We can apply the same expectation of negligible reference self-potential magnitudes to
325 our surveys at Rhone Glacier on the three successive days. We find that absolute liquid water
326 contents inferred from equation (4) generally fall well within the range of ~ 3 – 8% inferred
327 from our ground-truth hand tests. We can therefore conclude that given careful emplacement
328 of the reference electrode, the simple empirical relationship between self-potential magnitudes,
329 discharge and liquid water content is robust not only in a laboratory setting (Kulesa et al.,
330 2012), but also for application to in-situ snowpacks. The self-potential method therefore shows
331 considerable promise as a non-intrusive snow-hydrological sensor.

332

333 **5. Objective 2: Self-potential sensitivity to uncertainty in snow properties**

334 We evaluate the sensitivity of calculated liquid water contents to both individual and combined
335 parameter uncertainties. For each parameter a range of uncertainty values was created, with the

336 respective minima and maxima approximately twice that of the uncertainty (Table 1). Repeat
337 water content calculations were carried out initially by changing each parameter individually
338 for a range of values between the respective minima and maxima. The results cluster broadly
339 in three categories, including the zeta potential (up to ~ 20 % change in liquid water content
340 within the 50 % uncertainty range), followed by grain diameter, survey area width, electrical
341 conductivity, snow depth and snow density (~ 3 – 4 % change) and bulk discharge, and self-
342 potential (2 % change) (Fig. 6). These three categories readily reflect our knowledge of or
343 ability to measure in-situ the respective parameters, with surprisingly low sensitivity to cross-
344 sectional area despite our simplistic calculation and significant inherent assumptions (i.e. 1 – 4
345 in Section 4). Self-potential magnitudes are readily measured in the field with minimum
346 uncertainty (Fig. 6), although the strongly enhanced sensitivity to the zeta potential highlights
347 the need for focused research to tightly constrain possible values of this parameter in in-situ
348 snow packs.

349 While this gives a good indication of the parameters to which water content calculations
350 are most sensitive, it does not indicate possible feedbacks between parameters. Feedbacks were
351 therefore evaluated by calculating liquid water contents for all possible combinations of the
352 best estimates and minimum and maximum parameter values (Table 1), giving over 6500
353 solutions (Fig. 7). The minimum and maximum outputs were then adopted as the lower and
354 upper uncertainty bounds (Fig.3). Due to the large potential uncertainty in the zeta potential,
355 the sensitivity range was arbitrarily set to ± 50 % for illustrative purposes (Section 4).

356 Despite our consideration of extreme potential error bounds, calculated uncertainties in
357 liquid water contents are restricted to a relatively small range (~ 20 % for large assumed
358 uncertainty in the zeta potential, and ~ 3 – 4 % otherwise) at both Rhone Glacier and
359 Jungfrauoch Glacier, and absolute values remain within the pendular regime where water
360 bodies in the pore space remain isolated. At the latter site the daily evolution of liquid water

361 contents thus is well captured even if uncertainty is taken into account (Fig. 5b), and likewise
362 at Rhone Glacier calculated liquid water contents plus uncertainties still fall within the range
363 of field measurements (Fig. 5a). Our inferences thus not only support Kulesa et al.'s (2012)
364 notion that existing snow hydrological relationships are robust for modelling purposes, but also
365 suggest that they may apply to in-situ field surveys. These inferences can also provide an
366 explanation for the relatively large self-potential magnitudes generated by relatively low bulk
367 discharge at Jungfrauoch Glacier (Fig. 2). Because we did not observe or infer any consistent
368 or statistically-significant differences between Rhone Glacier and Jungfrauoch Glacier in
369 dielectric permittivity (ϵ), zeta potential (ζ), saturation ($S_w S_e^{-n}$), electrical conductivity (σ_w) or
370 cross-sectional area (A), the only remaining parameter that could facilitate the observed relative
371 difference is permeability (k). Indeed, using an average snow density of 564 kg m^{-3} , the
372 differences in mean snow grain sizes between Rhone Glacier ($1.5 \times 10^{-3} \text{ m}$) and Jungfrauoch
373 Glacier ($1 \times 10^{-3} \text{ m}$) translate into respective permeabilities of $9.7 \times 10^{-5} \text{ m}^2$ and $4.3 \times 10^{-5} \text{ m}^2$.
374 The relatively reduced permeability of Jungfrauoch Glacier's accumulation-area snow-pack
375 therefore likely supported the presence of self-potential magnitudes that were markedly
376 elevated relative to Rhone Glacier's ablation-area snow-pack (equation (4)). This inference
377 emphasises the sensitivity of the self-potential method to permeability as a fundamental snow-
378 hydrological property, along with its observed sensitivity to bulk melt water discharge and
379 inferred sensitivity to liquid water content.

380

381 **6. Synthesis and conclusions**

382 The ability of the electrical self-potential method to sense meltwater flow in in-situ snowpacks
383 is unique, where self-potential magnitudes scale directly with discharge and are zero in the
384 absence of flow. The scaling factor [\(right side of equation \(4\)\)](#) depends principally on the liquid
385 water content of the snowpack, its permeability and the water chemistry (Kulesa et al., 2012).

386 We have shown here that diurnal variations in the liquid water content of in-situ snowpacks
387 can be derived from electrical self-potential data and bulk discharge measurements with a
388 simple lysimeter. This derivation was subject to four key assumptions (Section 4) which we
389 now examine in turn to identify what, if any, constraints arise for future applications.

390 The Reynolds number (Re) is a common measure of the mode of fluid flow through
391 porous media, as discussed in a relevant cryospheric context by Kulesa et al. (2003a)

392

$$Re = \frac{\rho_s v L}{\eta} \quad (9)$$

393

394 where v and L are respectively characteristic fluid flow velocity (in m s^{-1}) and characteristic
395 length scale of flow (in m), and ρ_s and η are respectively snow density (in kg m^{-3}) and dynamic
396 viscosity (in Pa s). To a first approximation the transition from laminar to turbulent flow
397 nominally occurs when $Re \approx 10$, although laminar flow can persist at much higher values of Re
398 (for comparison, in open channels transition occurs at $Re \approx 2300$). For our purposes v can be
399 assumed to correspond to the average linear velocity of flow, $v = Q A^{-1} n^{-1}$, where n is effective
400 porosity (ratio of snow and ice densities). In porous media such as snow L corresponds to the
401 average pore diameter, and in the absence of direct evidence is assumed to be equal to grain
402 size. Where snow is denser than $\sim 490 \text{ kg m}^{-3}$, such as that at our study sites (average ~ 564
403 kg m^{-3}), grain size is expected to be larger than pore diameter (Schneebeli and Sokratov, 2004).
404 This assumption is therefore likely ~~in practice~~ an overestimation of pore diameter. For the
405 respective snow properties and their uncertainties reported in Table 1 values of Re between \sim
406 $0. \leq 1$ and 51~~~50.7~~ are obtained, with a best estimate of $Re \approx 1.1$. These values pertain to times
407 of highest measured meltwater discharge when the Reynolds number is likely be greatest.
408 Despite the unrealistically large uncertainty bounds considered in Table 1, and the
409 overestimation of pore diameter (L) and associated inflation of the Reynolds number (equation

410 (9)), we can therefore conclude that meltwater flow in our snowpacks was laminar. The
411 absolute and relative inclinations of the snow surface and base will vary to different degrees
412 within different field areas, thus generating differences in discharge and potentially preferential
413 flow. Indeed, it is an exciting attribute of self-potential measurements that they will, in practice,
414 aid to delineate such differences in meltwater flow.

415 Persistent meltwater runoff at the snow surface is uncommon, and meltwater flow
416 through underlying soils or ice will normally be negligible or small compared to flow through
417 or at the base of snowpacks. We have also shown that the [estimation of snow properties, such](#)
418 [as liquid water content, from inversion-of-self-potential data for snow properties such as liquid](#)
419 [water content](#) is insensitive to the area of snowpack contributing meltwater flow to the
420 measured signals. Uncertainties in the area of origin of water contributing to measured bulk
421 discharges and thus measured self-potential data are not therefore expected to be a major
422 hindrance to future applications of the self-potential method to snow problems. We have also
423 shown that with the exception of the zeta potential, sensitivity to uncertainties in the snow
424 properties governing the relationship between self-potential data and liquid water contents are
425 small (~ 3-4% in our feasibility study). Future work must ascertain to what extent longer-term
426 monitoring studies are affected by the preferential elution of ions and the associated impacts
427 on meltwater pH, EC and thus the zeta potential. Even if such effects were found to be of
428 concern, meltwater EC and pH are readily monitored in-situ with automated probes and could
429 be measured alongside self-potential data at a calibration location, and subsequently be
430 assimilated in snow models. [Being able to characterise LWC over significant spatial areas is](#)
431 [limited to the spatial distribution and density of possible electrode placement. However, the](#)
432 [robustness of the estimation means that in practice SP measurements at several points within](#)
433 [the area of interest can in the future make reliable interpolations between measurements in](#)
434 [space and time.](#)

435 The final consideration focused on the assumption that the spatial pattern of self-
 436 potential magnitudes, measured during the day across our survey areas, was due to temporal
 437 changes in the liquid water content of the snowpack. This assumes that any spatial pattern due
 438 to elevation changes between the bottom and top of our survey areas is comparatively small
 439 and indeed negligible. Kulesa et al. (2003a) showed that elevation-driven changes in the self-
 440 potential fields measured between upstream (Ψ_{up}) and downstream (Ψ_{down}) locations (z_{up} , z_{down})
 441 can be approximated by

$$\Psi_{up} - \Psi_{down} = -\frac{\varepsilon\zeta}{\eta\sigma_w} S_w (z_{up} - z_{down}), \quad (10)$$

443 here translated to our notation and adjusting for meltwater saturation according to equation (2).
 444 Even for the maximum daily values of saturation inferred from our measurements the
 445 elevation-driven spatial pattern has small magnitudes, estimated to be ~ -16.0 mV and -8.4 mV
 446 respectively for Jungfrauoch Glacier and Rhone Glaciers. These values are an order of
 447 magnitude smaller than daily changes measured at the two glaciers (Fig. 2) and are therefore
 448 considered to be insignificant for the purpose of the present feasibility study. In similar future
 449 applications the relevance of such spatial changes should be assessed on a case by case basis,
 450 and would in fact readily be incorporated into quantitative inferences of snow properties from
 451 self-potential data where they are of concern.

453 Overall our findings imply that in principle, self-potential data could be inverted for
 454 spatial or temporal variations in any one desired parameter (i.e. discharge, liquid water content,
 455 permeability or water chemistry), if independent estimates of the respective remaining
 456 parameters are available. Self-potential data are therefore well suited for assimilation in snow
 457 models along with meteorological and snowpack observations. We have shown in previous
 458 cryospheric applications that self-potential monitoring is readily effected with autonomous

459 arrays of low-cost non-polarising electrodes connected to a high-impedance data logger
460 (Kulesa et al., 2003a, 2003b, 2012). In operational practice for instance, 2-D vertical arrays of
461 electrodes and data loggers could be installed along with meteorological stations and upward-
462 looking radar instrumentation, where the latter is used to monitor snow structure and 1-D liquid
463 water contents. Assimilation of self-potential data along with complementary meteorological
464 and radar data could then facilitate unique insights into daily and longer-term variations in 2-
465 D vertical, lateral and preferential meltwater flows, or in liquid water contents. We conclude
466 that the integration of self-potential measurements into existing snow measurement and data
467 assimilation routines shows considerable promise in supporting a reduction of uncertainty in
468 quantifying snow-atmosphere energy exchanges, or in predictive modelling used in operational
469 snow forecasting.

470

471 **Acknowledgements**

472 This work was carried out while SST was working at VAW ETH Zurich within the Swiss
473 National Science Foundation project; Accelerated release of persistent organic pollutants
474 (POPs) from Alpine glaciers, Research Grant 200021_130083/1 BAFU, with support of the
475 Swiss Federal Office for the Environment (FOEN/BAFU). We would like to thank two
476 anonymous reviewers whose comments improved clarity of the manuscript and Martin Funk
477 and VAW for hosting and supporting the work and for extensive support for fieldwork. Also
478 thanks to Fabian Wolfsperger at WSL-Institute for Snow and Avalanche Research SLF and
479 Ludovic Baron at UNIL Université de Lausanne for providing equipment for fieldwork. Thanks
480 to Jordan Mertes, Celia Lucas, Saskia Grindreaux, Barbara Reyes-Trüssel and Moira
481 Thompson for invaluable help in the field.

482

483

484

485

486 **References**

487 [Albert, M., and Krajewski, G.: A fast, physically based point snowmelt model for use in](#)
488 [distributed applications, Hydrol. Processes, 12, 1809–1824, doi:10.1002/\(SICI\)1099-](#)
489 [1085\(199808/09\)12:10/11<1809::AID-HYP696>3.0.CO;2-5, 1998.](#)

490 Barnett, T.P., Adam, J.C., and Lettenmaier, D.P.: Potential impacts of a warming climate on
491 water availability in snow-dominated Regions, *Nature*, 438(17), 303-309, doi:
492 10.1038/nature04141, 2005.

493 Campbell, F.M.A., Nienow, P.W., and Purves, R.S.: Role of the supraglacial snowpack in
494 mediating meltwater delivery to the glacier system as inferred from dye tracer investigations,
495 *Hydrol. Process.*, 20(4), 969-985, doi: 10.1002/hyp.6115, 2006.

496 Colbeck, S.C., Akitaya, E., Armstrong, R., Gubler, H., Lafeuille, J., Lied, K., McClung, D.,
497 and Morris, E.: The International Classification for Seasonal Snow on the Ground: The
498 International Commission on Snow and Ice of the International Association of Scientific
499 Hydrology, 1990.

500 Corry, C.E., De Moully, G.T. and Gerety, M.T.: *Field Procedure Manual for Self-Potential*
501 *Surveys*, Zonge Engineering and Research Organization Publishing, Arizona USA, 1983.

502 Darnet, M., Marquis, G., and Sailhac, P.: Estimating aquifer hydraulic properties from the
503 inversion of surface streaming potential (SP) anomalies, *Geophys. Res. Lett.*, 30(13), 1679,
504 doi: 10.1029/2003GL017631, 2003.

505 Denoth, A.: An electronic device for long-term snow wetness recording, *Ann. Glaciol.*, 19,
506 104-106, 1994.

507 Doherty, R., Kulesa, B., Ferguson, A.S., Larkin, M.J., Kulakov, L.A., and Kalin, R.M.: A
508 microbial fuel cell in contaminated ground delineated by electrical self-potential and

509 normalized induced polarization data, *J. Geophys. Res.*, 115, G00G08, doi:
510 10.1029/2009JG001131, 2010.

511 Drzymala, J., Sadowski, Z., Holysz, L., and Chibowski, E.: Ice/water interface: Zeta potential,
512 point of zero charge, and hydrophobicity, *J. of Colloid Interf. Sci.* 200, 229-243, 1999.

513 Essery, R., Morin, S., Lejeune, Y., and Ménard C.B.: A comparison of 1701 snow models using
514 observations from an alpine site, *Adv. Water Resour.* 55, 131-148, doi:
515 10.1016/j.advwatres.2012.07.013, 2013.

516 Fierz, C., Armstrong, R.I., Durand, Y., Etchevers, P., Greene, E., McClung, D.M., Nishimura,
517 K., Satyawali, K., and Sokratov, S.A.: The International Classification for Seasonal Snow on
518 the Ground. IHP-VII Technical Documents in Hydrology N°83, IACS Contribution N°1,
519 UNESCO-IHP, Paris, 2009.

520 French, H. K., Binley, A., Kharkhordin, I., Kulesa, B. and Krylov, S.S.: Permafrost and
521 snowmelt, in *Applied Hydrogeophysics*, Vereecken H. et al. (eds), 195–232, Springer, New
522 York, 2006.

523 Heilig, A., Eisen, O., and Schneebeli, M.: Temporal observations of a seasonal snowpack using
524 upward-looking GPR, *Hydrol-Process*, 24(22), 3133-3145, doi:10.1002/hyp.7749,2010.

525 ~~Jouniaux, L., Maineult, A., Naudet, V., Pessel, M. and Silliac, P.: Review of self potential~~
526 ~~methods in hydrogeophysics, *C. R. Geoscience* 341(10–11), 928–936, doi:~~
527 ~~10.1016/j.erte.2009.08.008, 2009.~~

528 Jougnot, D., Linde, N., Revil, A., Doussan, C.: Derivation of soil-specific streaming potential
529 electrical parameters from hydrodynamic characteristics of partially saturated soils, *Vadose*
530 *Zone J.* 11. doi:10.2136/vzj2011.0086, 2012.

531 Kallay, N., Cop, A., Chibowski, E., and Holysz, L.: Reversible charge of ice-water interface,
532 II: Estimation of equilibrium parameters. *J. Colloid Interf. Sci.*, 259, 89-96, doi:
533 10.1016/S00219797(02)00179-0, 2003.

534 Kulesa, B. A critical review of the low frequency electrical properties of ice sheets and
535 glaciers, *JEEM* 12(1), 23-36, doi: 10.2113/JEEG12.1.23, 2007.

536 Kulesa, B., Hubbard, B.P., and Brown, G.: Cross-coupled flow modelling of coincident
537 streaming and electrochemical potentials, and application to subglacial self-potential (SP) data,
538 *J. Geophys. Res.*, 108(B8), 2381, doi: 10.1029/2001JB001167, 2003a.

539 Kulesa, B., Hubbard, B.P., and Brown, G.: Earth tide forcing of glacier drainage, *Geophys.*
540 *Res. Lett.*, 30(1), doi: 10.1029/2002GL015303, 2003b.

541 Kulesa, B., Chandler, D.C., Revil, A., and Essery, R. L. H.: Theory and numerical modelling
542 of electrical self-potential (SP) signatures of unsaturated flow in melting snow, *Water Resour.*
543 *Res.* 48, W09511, doi: 10.1029/2012WR012048, 2012.

544 Linde, N., Revil, A., Bolève, A., Dagès, C., Castermant, J., Susli, B. and Voltz, M.: Estimation
545 of the water table throughout a catchment using self-potential and piezometric data in a
546 Bayesian framework, *J. of Hydrol.* 334, 88-98, doi: 10.1016/j.jhydrol.2006.09.027, [2007](#).

547 Livneh, B., Xia, Y., Mitchell, K.E., Ek, M.B., and Lettenmaier, D.P.: Noah LSM Snow Model
548 Diagnostics and Enhancements, *J. Hydrometeorol.*, 11, 721–738, doi: 10.1175/2009JHM1174.1,
549 2010.

550 Meyer, T. and Wania, F.: Organic contaminant amplification during snow melt, *Water Res.*
551 42(8-9), 1847-1865, doi:10.1016/j.watres.2007.12.016, 2008.

552 Meyer, T., Lei, Y.D. and Wania, F.: Organic contaminant release from melting snow. 1.
553 Influence of chemical partitioning, *Environ. Sci. Technol.* 43(3), 657-662, doi:
554 10.1021/es8020217, 2009.

555 Mitterer, C., Heilig, A., Schweizer, J., and Eisen, O.: Upward-looking ground-penetrating radar
556 for measuring wet-snow properties, *Cold Reg. Sci. Technol.*, 69(2-3), 129-138, doi:
557 10.1016/j.coldregions.2011.06.003. 2011.

558 Petiau, G.: Second generation of lead-lead chloride electrodes for geophysical applications,

559 Pure and Appl. Geophys., 157(3), 357-382, doi: 10.1007/s000240050004, 2000.

560 Revil, A., Schwaeger, H., Cathles, L.M. and Manhardt, P.: Streaming potential in porous
561 media. II: Theory and application to geothermal systems, J. Geophys. Res., 104, 20,033–
562 20,048, doi: 10.1029/1999JB900090, 1999.

563 Revil, A., Naudet, V., Nouzaret, J., and Pessel, M.: Principles of electrography applied to self-
564 potential electrokinetic sources and hydrogeological application, Water Resour. Res., 39(5), 1-
565 14, doi: 10.1029/2001WR000916, 2003.

566 Revil, A., Titov, K., Doussan, C., and Lapenna, V.: Application of the self-potential method
567 to hydrological problems, in: H. Vereecken, A. Binley, G. Cassiani, A. Revil, and K. Titov
568 (eds.), Applied Hydrogeophysics, Springer, Netherlands, 255-292, 2006.

569 Revil, A., Linde, N., Cerepi, A., Jougnot, D., Matthäi, S. and Finsterle, S.: Electrokinetic
570 coupling in unsaturated porous media, J. of Colloid Interf. Sci. 313(1), 315-327, doi:
571 10.1016/j.jcis.2007.03.037, 2007.

572 Schmid, L., Heilig, A., Mitterer, C., Schweizer, J., Maurer, H., Okorn, R., and Eisen, O.:
573 Continuous snowpack monitoring using upward-looking ground-penetrating radar technology,
574 J. Glaciol., 60(221), 509-525, doi: 10.3189/2014JoG13J084, 2014.

575 [Schneebeli, M. and Sokratov, S.A.: Tomography of temperature gradient metamorphism of](#)
576 [snow and associated changes in heat conductivity, Hydrol. Process. 18, 3655-3665, doi:](#)
577 [10.1002/hyp.5800, 2004.](#)

578 Shimizu, H.: Air permeability of deposited snow. Low Temperature Science Series A 22, 1-
579 32, 1970.

580 Sill, W.R.: Self-potential modeling from primary flows, Geophysics 48, 76–86, doi:
581 10.1190/1.1441409, 1983.

582 Thompson, S.S., Kulesa, B. and Luckman, A.: Integrated electrical resistivity tomography
583 (ERT) and self-potential (SP) techniques for assessing hydrological processes within glacial
584 lake moraine dams, *J. Glaciol.*, 58 (211), 1-10, doi: 10.3189/2012JoG11J235, 2012.

585 Wever, N., Fierz, C., Mitterer, C., Hirashima, H. and Lehning, M.: Solving the Richards
586 Equation for snow improves snowpack meltwater runoff estimations in detailed multi-layer
587 snowpack model, *The Cryosphere*, 8(1), 257-274, doi: 10.5194/tc-8-257-2014, 2014.

588 Williams, M.W., Cline, D., Hartman, M. and Bardsley, T.: Data for snowmelt model
589 development, calibration and verification at an alpine site, Colorado Front Range, *Water*
590 *Resour. Res.* 35 (10), 3205-3209, doi: 10.1029/1999WR900088, 1999.

591 Williams, M. W., Erickson, T. A., and Petzelka, J. L.: Visualising meltwater flow through
592 snow at the centimetre-to-metre scale using a snow guillotine, *Hydrol. Process.* 24 (15),
593 2098-2110, doi: 10.1002/hyp.7630, 2010.

594 **TABLES AND FIGURES**

595

596 **Table 1:** Best estimate of each parameter for Rhone Glacier SP (Day 2) and relative assumed
 597 uncertainty and sensitivity ranges. The sensitivity ranges are based on the measurement
 598 accuracy of each measured parameter or the confidence of estimates parameters. The
 599 uncertainty ranges are exaggerated from the sensitivity values to highlight the effect of poor
 600 measurement or estimation. .

601

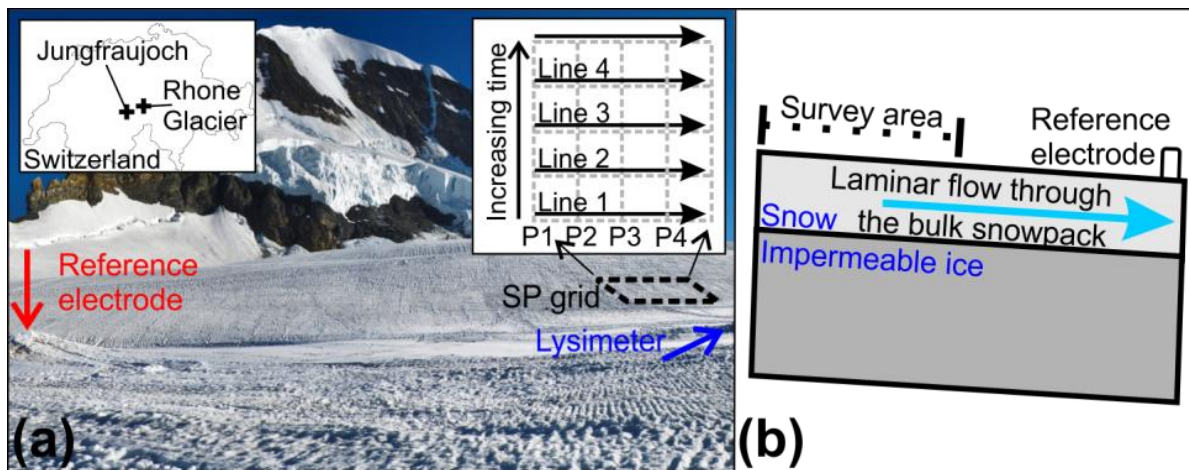
<u>Measured / estimated parameters</u>	<u>Best estimate</u>	<u>Uncertainty range</u>	<u>Sensitivity range</u>
Self-potential ψ_m (V)	Variable	$\psi_m \pm 40\%$	$\psi_m \pm 20\%$
Discharge Q ($m^3 s^{-1}$)	Variable	$Q \pm 40\%$	$Q \pm 20\%$
Electrical conductivity σ_w ($S m^{-1}$)	5×10^{-6}	$10^{-7} - 10^{-4}$	$\sigma_w \pm 5 \times 10^{-7}$
Zeta potential ζ (V)	-1×10^{-5}	$10^{-4} - 10^{-6}$	$\zeta \pm 50\%$
Permeability from;			
Grain diameter d (m)	0.00175	$d \pm 0.001$	$d \pm 0.0005$
Density ρ ($kg m^3$)	555.5	$\rho \pm 140$	$\rho \pm 70$
Cross sectional area from;			
Width w (m)	12.5	$w \pm 10$	$w \pm 5$
Depth dp (m)	1.45	$dp \pm 1$	$dp \pm 0.2$

602

<u>Measured / estimated parameters</u>	<u>Best estimate</u>	<u>Sensitivity range</u>	<u>Uncertainty range</u>
<u>Self-potential ψ_m (V)</u>	<u>Variable</u>	<u>$\psi_m \pm 20\%$</u>	<u>$\psi_m \pm 40\%$</u>
<u>Discharge Q ($m^3 s^{-1}$)</u>	<u>Variable</u>	<u>$Q \pm 20\%$</u>	<u>$Q \pm 40\%$</u>
<u>Electrical conductivity σ_w ($S m^{-1}$)</u>	<u>5×10^{-6}</u>	<u>$\sigma_w \pm 5 \times 10^{-7}$</u>	<u>$10^{-7} - 10^{-4}$</u>
<u>Zeta potential ζ (V)</u>	<u>-1×10^{-5}</u>	<u>$\zeta \pm 50\%$</u>	<u>$10^{-4} - 10^{-6}$</u>
<u>Permeability from;</u>			
<u>Grain diameter d (m)</u>	<u>0.00175</u>	<u>$d \pm 0.0005$</u>	<u>$d \pm 0.001$</u>
<u>Density ρ ($kg m^3$)</u>	<u>555.5</u>	<u>$\rho \pm 70$</u>	<u>$\rho \pm 140$</u>
<u>Cross sectional area from;</u>			
<u>Width w (m)</u>	<u>12.5</u>	<u>$w \pm 5$</u>	<u>$w \pm 10$</u>
<u>Depth dp (m)</u>	<u>1.45</u>	<u>$dp \pm 0.2$</u>	<u>$dp \pm 1$</u>

603

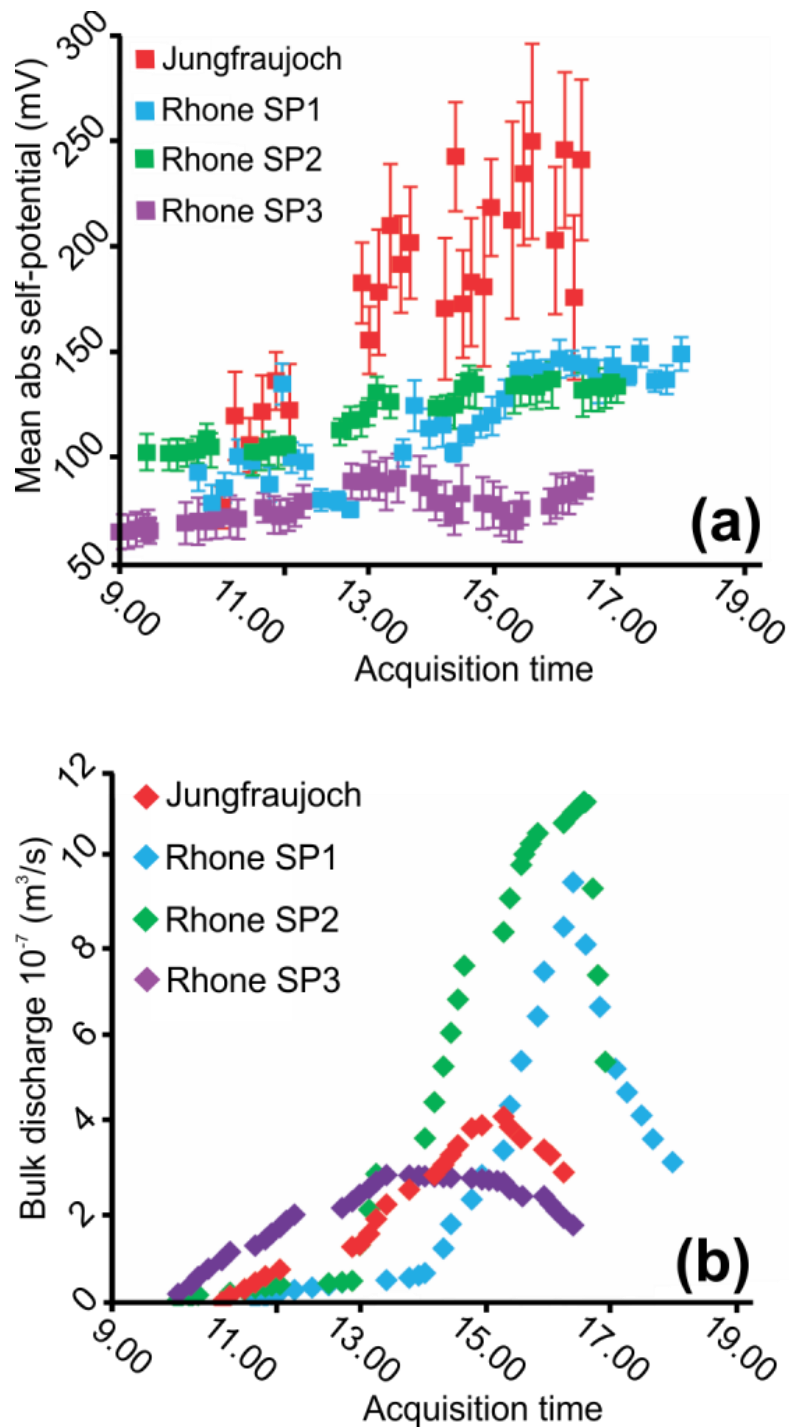
604



605

606 **Figure 1:** (a) Example survey set up, SP grid 25x25m. Insert left show the location of both
607 fieldsites. Insert right illustrates the self-potential survey design; to provide each self-potential
608 data value, a profile of 25 data points (P1, P2, etc.) was collected (Line 1, Line 2, etc.),
609 perpendicular to assumed bulk water flow. (b) Schematic of the self-potential experiment
610 developed by Kulesa et al. (2012) for the situ snowpack surveys.

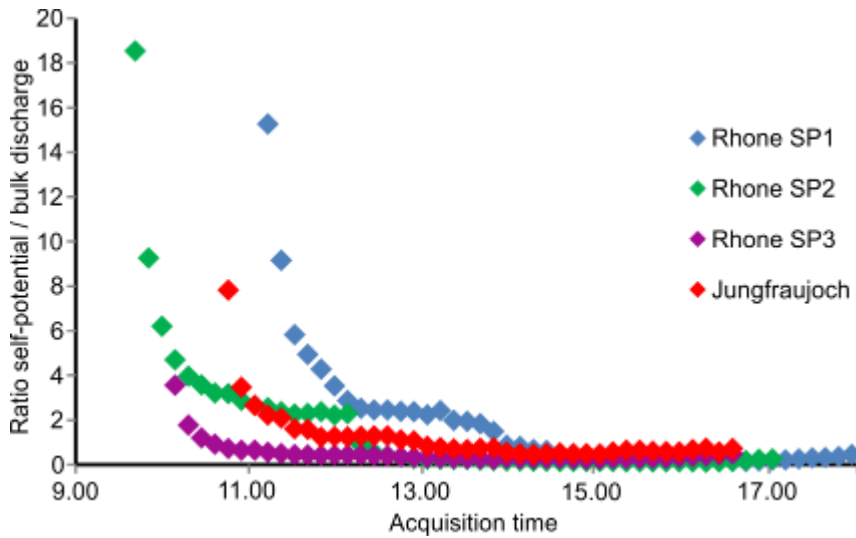
611



612

613 **Figure 2:** Time series of (a) bulk self-potential measurements and (b) bulk discharge
 614 measurements for the three Rhone Glacier surveys and the Jungfraujoch Glacier survey. Each
 615 self-potential data point represents the mean value of a profile (consisting of 25 data points);
 616 the error bars illustrates the variability over each profile. Bulk discharge was measured over
 617 each profile by the lysimeter.

618

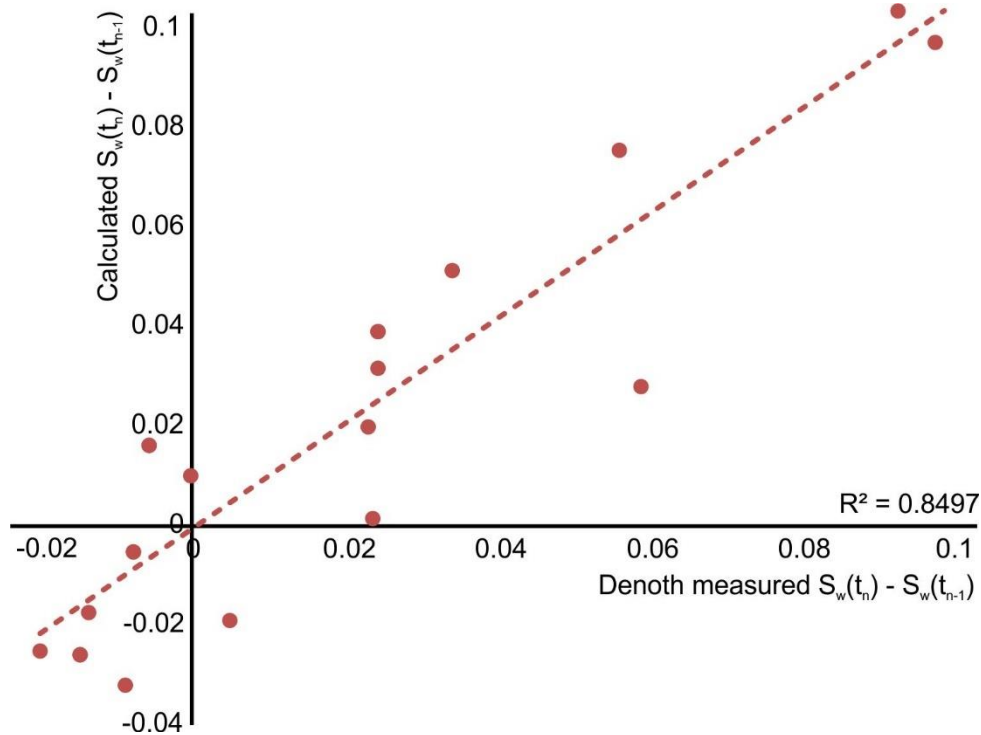


619

620 **Figure 3:** Ratio between self-potential (V) and bulk discharge ($\text{m}^3 \text{s}^{-1}$) for each of the four
 621 surveys through time, illustrating the ratio changes consistently over time.

622

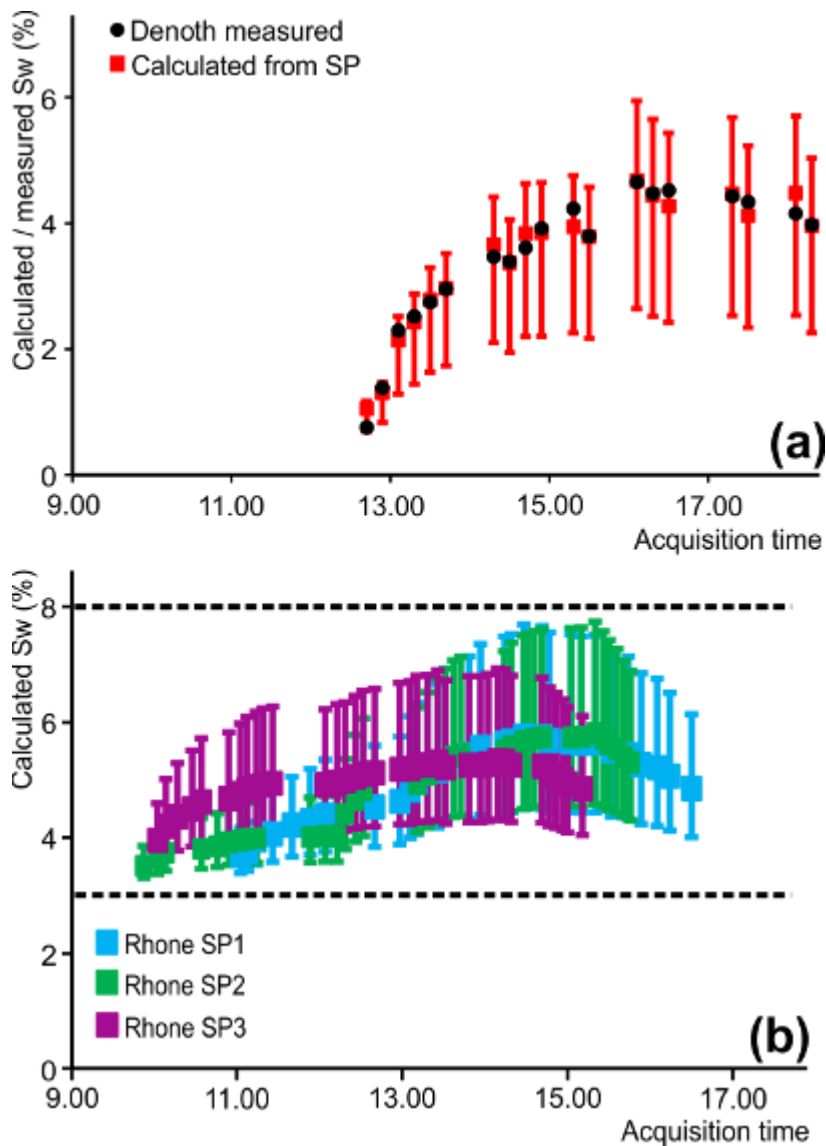
623



624

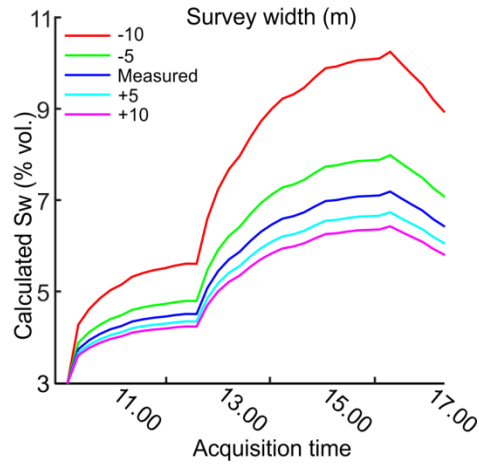
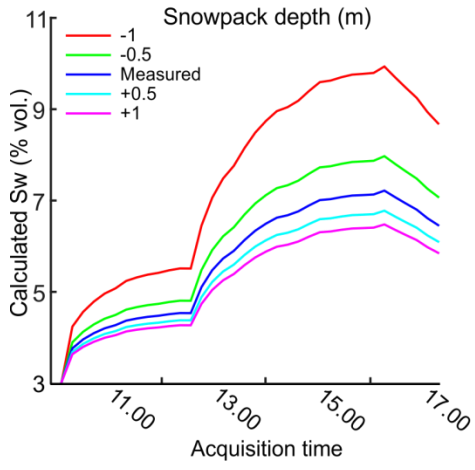
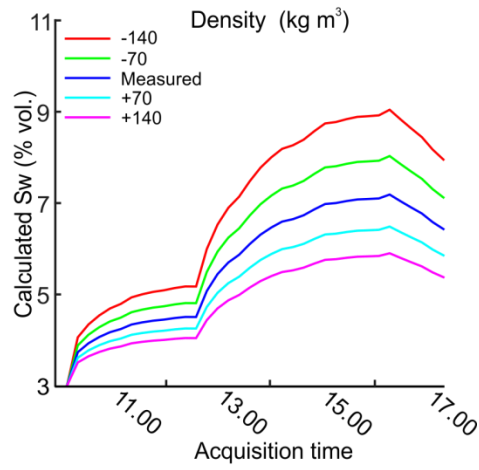
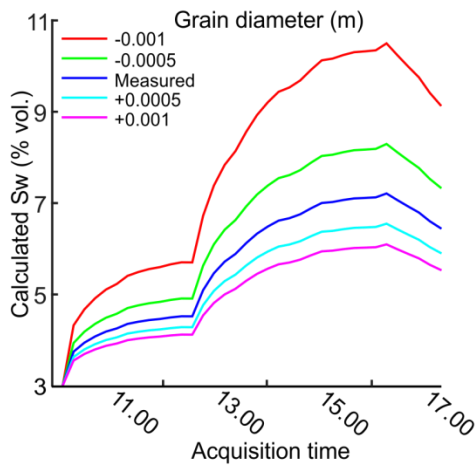
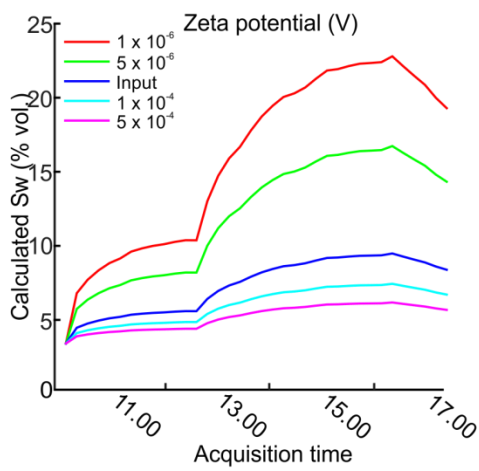
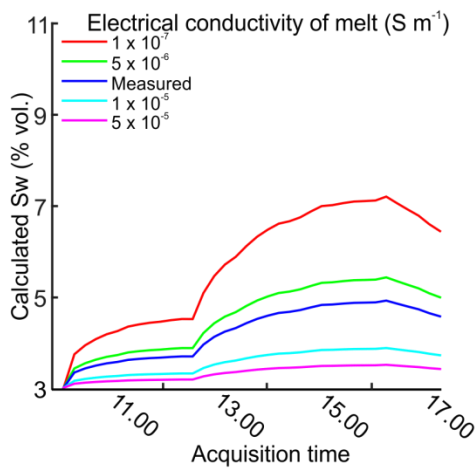
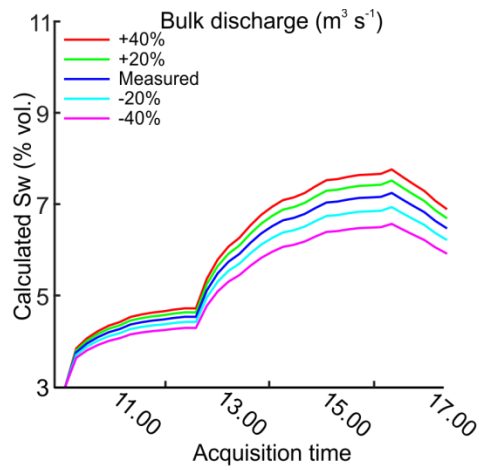
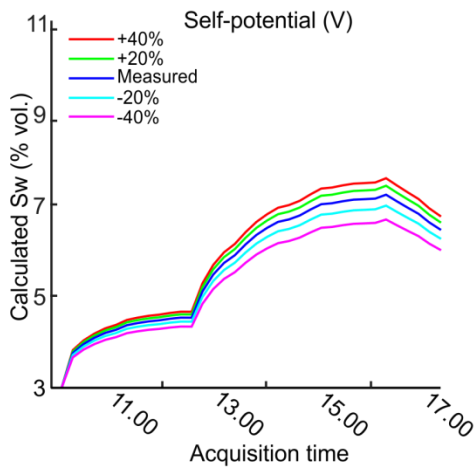
625 **Figure 4:** Temporal differences in S_w inferred from self-potential data against temporal
 626 differences in the Denoth measured S_w at Jungfrauoch Glacier, according to equation (5).

627

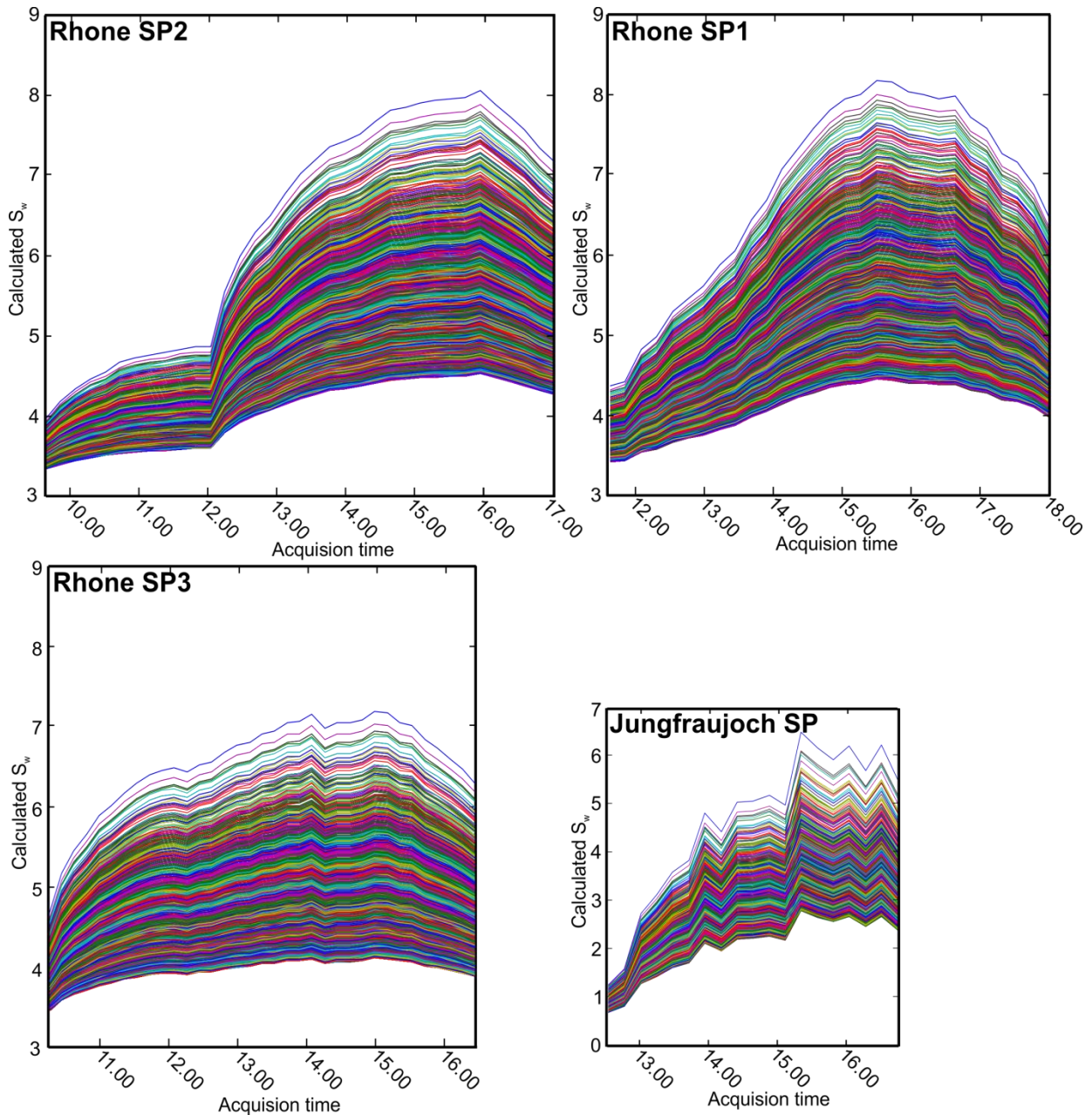


628

629 **Figure 5:** (a) Liquid water content calculated from equation 4 for the self-potential survey
 630 carried out at Jungfraujoch Glacier, with the corresponding Denoth measurements. The
 631 uncertainty range illustrates the minimum and maximum model results for the range of
 632 parameters (Table 1, Supplementary Material). (b) Liquid water content calculated from
 633 equation 4 for each of the three self-potential surveys carried out at Rhone Glacier. All results
 634 are within the range of liquid water content (% vol) estimated by the hand tests (black dashed
 635 lines in b).



637 **Figure 6:** S_w calculations for a range of values for each parameter. In each case the range is an
638 exaggerated uncertainty range (Table 1), highlighting the effect of each individual parameter
639 on the calculated S_w output, using Rhone Glacier SP2 as an example.
640



641
642 **Figure 7:** Full sensitivity analysis for each of the four data sets. Each graph shows the full
643 range of calculated liquid water content (S_w) values of every combination of minimum, best
644 estimate and maximum for each of the parameters.